Three-dimensional smoothed particle hydrodynamics modeling of preferential flow dynamics at fracture intersections on a high-performance computing platform

Deutsche Forschungsgemeinschaft

Lysander Bresinsky[1], Jannes Kordilla[1]

[1]University of Göttingen, Dept. of Applied Geology, Germany <lbresin@gwdg.de>

GEORG-AUGUST-UNIVERSITÄT GÖTTINGEN

I. Introduction

Free-surface flow at fracture intersections

- Fracture intersections are critical relay points along preferential flow paths and control the partitioning (i.e. dispersion) behavior
- Fracture networks in permeable porous media are subject to highly non-linear and rapid flow processes such as droplets, rivulets and (adsorbed) films, which are known to affect the bypass dynamics at fracture intersections (Kordilla, 2017)
- Volume-averaged models (e.g. Richards equation) with saturation-capillary-pressure relations (e.g. van Genuchten parameterization), do not account for complex flow mechanisms on a fracture- and fracture-network-scale
- Flows in unsaturated fractures are challenging to study numerically due to the presence of complex air-water interfaces

Objectives

- Develop a better understanding of the controlling factor of fracture intersections towards droplet partitioning and its implications for preferential flow
- Link geometric fracture characteristics and fluid properties to bypass dynamics
- Show the influence of horizontal offsets, various apertures and droplet volume on bypass efficiency via high performance smoothed particle hydrodynamics simulations

II. Methods

SPH implementation of the Navier-Stokes equation

- The foundations of SPH rely on the Navier-Stokes equations:

$$\frac{d\mathbf{v}}{dt} = -\frac{1}{\rho}\nabla p + \frac{\mu}{\rho}\nabla^2\mathbf{v} + \mathbf{g} \tag{1}$$

- Rewritten in SPH form:

$$\begin{aligned}\frac{d\mathbf{v}_i}{dt} = &- \sum_{j\epsilon fluid+solid}^{N} m_j \left(\frac{p_j}{\rho_j^2} + \frac{p_i}{\rho_i^2}\right)\mathbf{e}_{ij}\frac{dW(\mathbf{r}_{ij},h)}{dr_{ij}} \\ &+ 2\mu \sum_{j\epsilon fluid}^{N} m_j \frac{\mathbf{v}_{ij}}{\rho_i\rho_j r_{ij}}\frac{dW(\mathbf{r}_{ij},h)}{dr_{ij}} + \mathbf{g}_{sph} + \frac{1}{m_i}\sum_{j=1}^{N}\mathbf{F}_{ij} \\ &+ \mathbf{f}_\Gamma(\mathbf{r}_i,\mathbf{v}_i)\frac{m_k}{\rho_i\rho_k}(\mathbf{n_i}+\mathbf{n}_k)\cdot\frac{dW(\mathbf{r}_{ik},h)}{dr_{ik}}\end{aligned} \tag{2}$$

$\mathbf{v}_i$: particle velocity; t: time; p: pressure of particle i; m: particle mass; ρ: mass density; $\mathbf{r}$: position vector; h: weighting function range; W: weighting function; $\mathbf{g}$: gravitation; $\mathbf{F}$: particle interaction force; $\mathbf{f}_\Gamma$: volumetric source term; $\mathbf{n}$: normals of the interface; $\mathbf{e}_{ij}$: unit vector

- In the above equation the linearized viscosity term acts in between fluid particles only
- The interaction force is defined following Tartakovsky (2005) and Kordilla (2017) as a cubic-spline type function with short-range repulsive and long-range attractive components
- The variable slip boundary condition is imposed according to Pan (2014) via a volumetric source term $\mathbf{f}_\Gamma = \beta\mathbf{v}$, where $\mathbf{n}$ are the respective normals of the solid-fluid interface
- $\beta = 0$ (full slip) and $\beta = \infty$ (no-slip)
- Here β is chosen such that no-slip conditions are enforced
- Pressure is obtained from an equations of state (EOS)

$$p_i = \epsilon\left(\left[\frac{\rho_i}{\rho_0}\right]^\Gamma - 1\right) + p_0, \tag{3}$$

ρ_0: rest density; p_0: background pressure; ϵ: scaling constant

- Density is obtained from a kernel summation

$$\rho_i = \int_{j=1}^{N} m_j W(\mathbf{r}_{ij},h) \tag{4}$$

- Interparticle forces F_{ij} generate cohesion and adhesion

$$\mathbf{F}_{ij} = \begin{cases} s\cdot cos\left(\frac{1.5\pi}{3h}\,|\mathbf{r}_{ji}|\right)\frac{\mathbf{r}_{ji}}{|\mathbf{r}_{ji}|} \text{ for } |\mathbf{r}_{ji}| \le h \\ 0 \text{ for } |\mathbf{r}_{ji}| > h \end{cases} \tag{5}$$

s: interaction strength that can either describe solid-fluid s_{sf} or fluid-fluid interactions s_{ff}

III. Model calibration

- The static and dynamic contact angle control gravity-driven free-surface flow
- Critical calibration parameters: (a) fluid-fluid s_{ff}, (b) solid-fluid s_{sf} interaction strength, (c) speed of sound c_0 and (d) friction coefficient β

Surface tension

- Cohesive forces naturally created by s_{ff} and the EOS
- Pressure gradient ΔP of a simulated droplet under zero gravity
- Young-Laplace Law

$$\sigma = \frac{R_{eq}}{2}\Delta P \tag{6}$$

R_{eq}: radius at equilibrium; σ: surface tension; ΔP: pressure difference

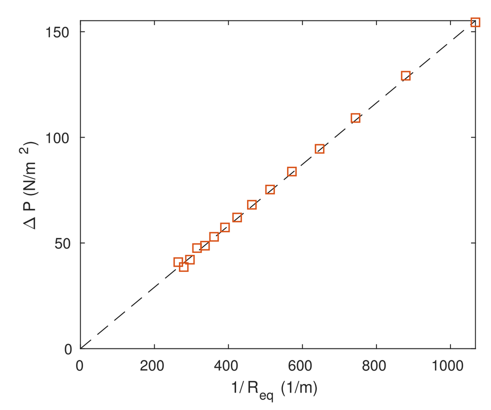

Figure 1: Surface tension

- A surface tension of $\sigma = 0.073\,\mathrm{N\,m^{-1}}$ was realized via $c_0 = 4.0\,\mathrm{m\,s^{-1}}$ and $s_{ff} = 3.5\times10^{-6}$

Static contact angle

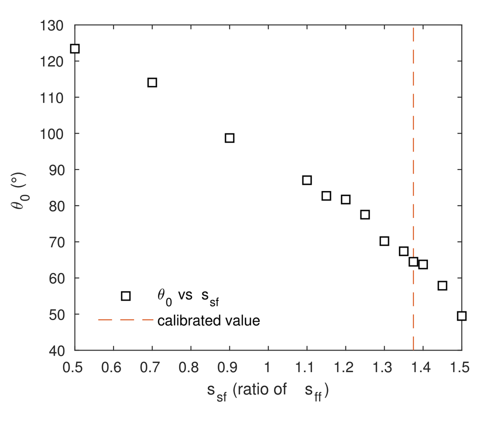

Figure 2: Contact angle

- Numerical dependence of static contact angle θ_0 and s_{sf} (fig. 2)
- Utilized to implement different wetting characteristics (fig. 3)
- A static contact angle of 65° is modeled (water droplets on acrylic glas matching laboratory goniometer measurements)

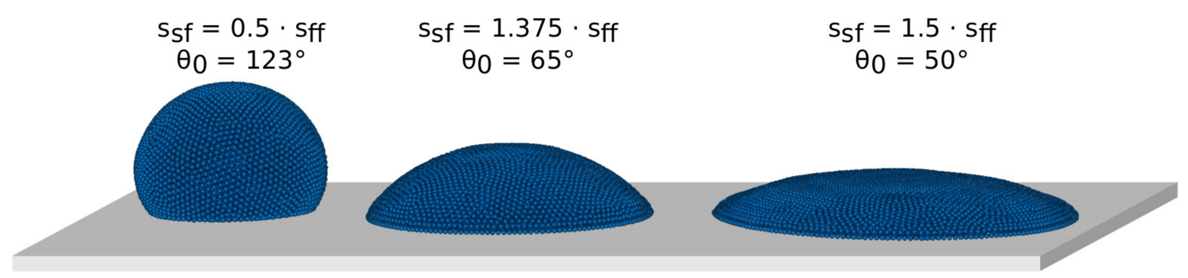

Figure 3: Contact angles formed by sessile droplets in SPH.

IV. Single-inlet partitioning dynamics

Model geometry

- Aperture d_f and offset d_{off} are adjusted by shifting the lower cube
- Fluid masses are measured in the domains R_1, R_2 and R_3 (fig. 5).

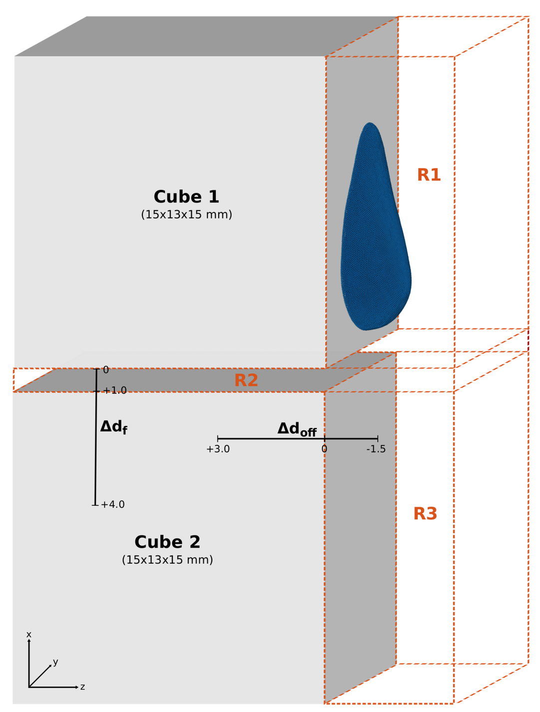

Figure 5: Morphology of the orthogonal fracture intersection in SPH.

General observations

- Small droplets may not overcome the sharp edge of the upper cube (Fig. 6a)
- Medium sized droplets have just enough gravitational energy to overcome the sharp edge, but are not able to hydraulically connect to the lower horizontal fracture wall (Fig. 6b)
- Large droplets have a more focused and enhanced momentum, as they flow at higher terminal velocities and assume an elongated shape, allowing the droplet to hydraulically connect to the lower horizontal fracture wall (Fig. 6c,d,e)

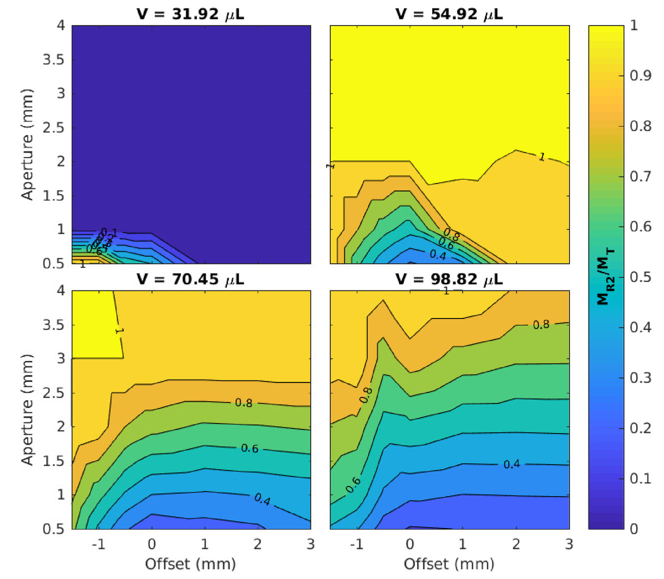

Figure 4: Total accumulated mass ratio of fluid in the horizontal fracture domain.

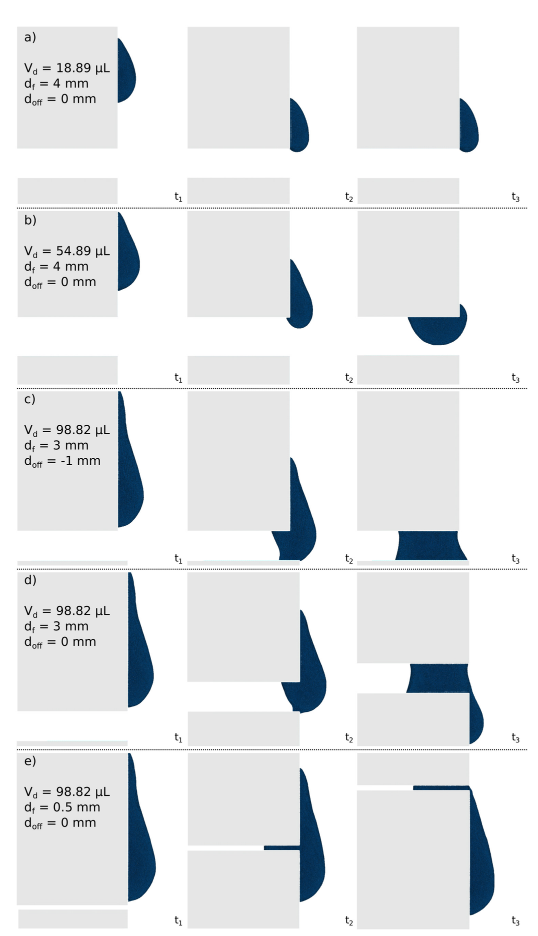
Figure 6: Example cases. Time advances from left to right.

Influence of fracture geometry

- Positive ($54\mathrm{\mu L} \le V < 88\mathrm{\mu L}$) and negative offsets inhibit vertical flow (fig. 4). Fluid that connects to the protruding lower horizontal fracture wall is decelerated and subject to a Washburn-type fracture inflow.
- Higher accumulation of water in the horizontal fracture domain with increasing aperture d_f ($V \ge 54\mathrm{\mu L}$)(fig. 4).
- Small droplets ($V < 54$) remain pinned above the intersection, but may hydraulically connect to the lower horizontal fracture wall (when d_f is very small)

Influence of droplet volume and height

- With increasing droplet size, the influence of interfacial forces with respect to gravitational forces decreases. Therefore, the capillary force pinning the droplet onto the fracture surface is dominating the force balance for smaller droplets
- Below a certain Bond number $Bo \approx 1.8$ (Fig. 7), a droplet will remain pinned on the upper vertical fracture wall

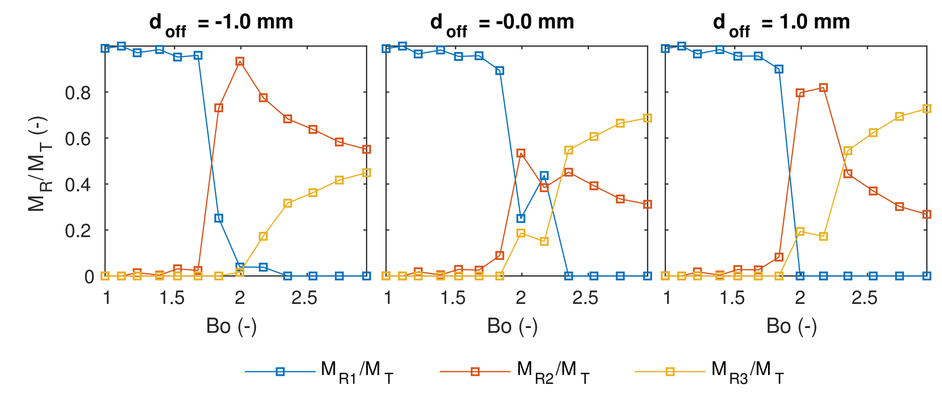

Figure 7: Mass ratio M_R/M_T in the domain R_1, R_2 and R_3 with respect to the Bond number Bo. An aperture of $d_f = 1.0\,\mathrm{mm}$ was applied.

- A linear dependence between the bypassing fluid mass and the ratio of droplet height and aperture d_f/h_d can be observed (fig. 8)

$$\frac{M_{R3}}{M_T} = \tau_1\frac{d_f}{h_d} + \tau_2, \tag{7}$$

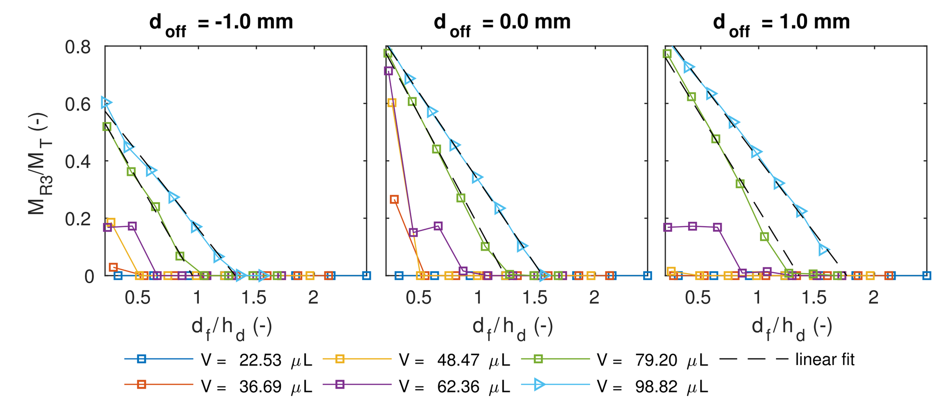

Figure 8: Mass ratio M_{R3}/M_T of the bypassing fluid with respect to aperture and droplet height d_f/h_d.

V. Conclusion & Outlook

- A three-dimensional Pairwise-Force Smoothed Particle Hydrodynamics model was applied in order to simulate gravity-driven multiphase flow at synthetic fracture intersections
- Significant differences in fluid dynamics at fracture intersections could be observed when minor changes to the geometry of fracture intersection or droplet volume were implemented

Outlook

- Derive an analytical correlation and interpretation of partitioning dynamics, droplet height and aperture
- Established scaling relationships in terms of Capillar and Bond numbers to characterize fluid-substrate combination (Podgorksi, 2001) may help to unify and generalize the results

Acknowledgement:
This work was funded by the Deutsche Forschungsgemeinschaft (DFG; German Research Foundation) under grant no. SA 501/26-1 and KO 53591/1-1.

References:
Kordilla (2017): Water Resour. Res. **(Early View)**; Podgorski (2001): Phys. Rev. Lett. **(87)**; Tartakovsky (2005): Phys. Rev. **(72)**; Pan (2014): J. Comput. Phys **(259)**